Responses to Referee #2:

In this work, Li et al. present single-particle aerosol mass spectrometry (SPAMS) measurements on the Tibetan Plateau. Measurements were taken over a month as part of an intensive campaign. In addition to SPAMS measurements, meteorological conditions were measured, as well as ozone and NOx. Almost 500,000 bi-polar, single-particle mass spectra were obtained. Spectra were subject to a clustering analysis. Air mass back trajectories were also calculated, and also were clustered. Two episodes of high particle concentrations are highlighted. From a cluster analysis of back trajectories, these episodes are from similarly sourced air, but they contain different fractions of particle types. The main difference is that there was more dust in Episode 1. Finally, the authors found relationships between the fraction of particles containing certain secondary aerosol markers and Ox and RH.This work is novel and is deserving of publication, but it requires major revisions in order to be published. See the major comments section for more details

Response: We sincerely appreciate all valuable comments and suggestions to our manuscript. We have carefully revised the relevant content. We do believe that the revised manuscript has been significantly improved after the revision. The point-to-point responses are shown, the modifications to the manuscript are marked in blue, and the revised text is underlined in italics. Attached please also find the marked-up manuscript with tracked changes.

Major Comments

1. There are many grammatical errors throughout this text. This reviewer strongly suggests that the authors carefully revise the manuscript to address these errors. Unfortunately, at this point, it makes it difficult to understand the author's interpretation of the results, and thus the paper suffers. Here are some examples from the abstract alone:

Response: All suggested typos and grammatical mistakes have been corrected. Meanwhile, the revised manuscript has been edited and proofread by a native English speaker. The critical revision has been shown in follows.

1. Line 19: "… which is a transport channel for pollutants from South Asia [to where?] during the pre-monsoon season."

Line 15-19:
"The unique geographical location of the Tibetan Plateau (TP) plays an important role in regulating global climate change, but the impacts of the chemical components and atmospheric processing on the size distribution and mixing state of individual particles are rarely explored in the southeastern margin of the TP, which is a transport channel for pollutants from South Asia to the TP during the pre-monsoon season."

2. Line 25: It is not clear what the "surroundings" means here, and the phrase "cross-border" here is either excessive or confusing.

Line 24-27:
"Most particle types were mainly transported from the surroundings of the sampling site and Sino-Myanmar border; but the air masses from northeastern India and Myanmar show a greater impact on the number fraction of BB (31.7%) and Dust (18.2%) types, respectively."

3. Line 27: I'm not sure what the "Besides" at the beginning of this sentence is referring to. I also think you should say either "episodes" or "events" here, but probably not "episodes events."

Line 28-31:
"Then, the two episodes with high particle concentrations showed that the differences in the meteorological conditions in the same trajectory clusters could cause significant changes in chemical components, especially the Dust and EC-aged types, which changed by a sum of 93.6% and 72.0%, respectively."

4. Line 29: The phrase "air clusters" is used here, but it has not been defined before, and it is not intuitive from the wording what it means.

Line 29:
We have exchanged the original clause "air clusters" for *"trajectory clusters"* in the revised version.

5. Line 30: I think you want to add a ", which" after "types" and a "," after "72%."

Line 30-31:
"especially the Dust and EC-aged types, which changed by a sum of 93.6% and 72.0%, respectively."

6. Line 34: I think "severed" is supposed to be "served."

Corrected.

2. Because there are many instances of grammatical errors throughout the text, the focus of the following comments will be of a general nature and will mainly be guided by the figures themselves; specific comments on the text in the main body of the paper will be withheld in anticipation of major revisions.

Response: The grammatical errors and unprofessional descriptions are thoroughly revised in this revised manuscript. The revised manuscript has been polished by a native English-speaking scientist.

3. The authors dedicate a lot of time in the results section interpreting the "size distributions." Unfortunately, it is difficult to interpret these results without some sense of the total aerosol size distribution (from an SMPS or OPC like

UHSAS, LAS, etc.). Your "size distribution," as presented, is sensitive to the detection efficiency of particles as a function of size. Furthermore, it may also be sensitive to particle shape. Both need to be accounted for prior to interpreting the size distribution.

Response: After consideration of the reviewer's comment, the descriptions of particle size distribution have been reduced. As shown in Section 3.2 (new Lines 270-297), the comparison and quantitative description of the size distribution of different types of particles have been deleted in the revised manuscript.

Line 270-297:

"The aerodynamic size distributions of all particle types are shown in Fig. 3. According to the characteristics of the average MS (Text S1 and Fig. S3), rich-K, BB, OC and EC-aged particles originated from the similar sources of vehicle emission or solid-fuel combustion. Their size distribution thus presents within a small-scale (~440 nm) (Fig. 3a). However, the relative percentage of each particle type is distinct with different size ranges, possibly due to the unique atmospheric processing. For example, as shown in Fig. 3b, the proportions of rich-K and BB types increases along with the increases in particle size from 200 to 420 nm but then decrease. OC and EC-aged types are mainly distributed in relatively small particle sizes, and their proportions gradually decrease when the size ranges become larger. Ammonium and Dust types are mainly distributed in large sizes of ~600 nm (Fig. 3a). The proportion of Ammonium particles gradually increases with the increase of particle size and peaks at 740 nm, the relatively large size distribution is ascribed to the intense atmospheric aging during regional transport (Text S1). The proportion of Dust particles gradually increases with a size > 560 nm and peaks at 1.48 μm. This is consistent with the fact that dust is a coarse particle, generally formed at the roadside and fly ash.

Compared with the total particle size distribution, the peak values of the six main particle types show minor differences (< 80 nm) during the two different episode periods (Fig. S10a). In Fig. S10b, a relatively high proportion of the rich-K and BB particles exhibit bimodal distributions, while peaks at < 300 nm are affected by the primary emissions and > 300 nm are associated with the aging process (Li et al., 2022b; Bi et al., 2011). Hence, the percentage of the six particle types distribute in wider size ranges during E2 than E1 due to the more intensive atmospheric aging. Relatively greater fluctuation for the large-size fractions (> 1.1 μm) could be explained by the low particle concentration (a number less than 20). It should be pointed out that further application of this method would require a co-located particle-sizing instrument to scale the size-resolved particle detection efficiency. Both particle composition and size-dependent are the predominant impacting factors on the particle detection efficiency of the SPAMS (Wenzel et al., 2003; Yang et al., 2017; Healy et al., 2013)."

In our study, the aerodynamic size range for SPAMS is 0.2-2.0 μm. A silicone dryer was also set up in front of the inlet system to avoid water vapor condensation which reduces the uncertainties in particle collection efficiency due to variable humidity (Matthew et al., 2008; Zhao et al., 2017). The above description has been supplemented in Section 2.2.

Line 139-141

"A hollow silicone dryer was installed in front of the inlet. This reduces the uncertainty of particle collection efficiency due to the changes of humidity in sampled airs."

According to the schematic diagram of the SPAMS (Fig. R3), the distance between two 532 nm lasers is known. In addition, the time of flight of the particle could be counted, while the particle velocities are thus calculated. Different sizes (i.e., 240, 320, 510, 740, 960 nm, 1.4 μm, and 2.0 μm) of standard polystyrene latex spheres (PSL) were used to calibrate the SPAMS. The calibration curve was developed as below.

$$y = C_1 + C_2x + C_3x^2 + C_4x^3$$

where y is the particle aerodynamic size; *x* is the particle velocity. The particle size calibration parameters (i.e., C_1, C_2, C_3, and C_4) were obtained under the inlet pressure of 2.40 Torr. The continuous velocity of the particles was converted into the corresponding vacuum aerodynamic diameter.

According to the information shown by Li et al. (2011), the main influencing factor that could cause the size deviation of the measured particles is the inlet pressure. The inlet pressure must be controlled within the range of ± 0.05 Torr as small as possible. During the sampling period, if the critical orifice is contaminated, the inlet pressure could be altered. To avoid this issue, we have regularly used the supersonic cleaner to remove the contamination in the critical orifice by soaking it in an ethanol solution. In addition, we have controlled the inlet pressure between 2.35 and 2.45 Torr to ensure the accuracy of the data obtained by SPAMS during the entire observation period.

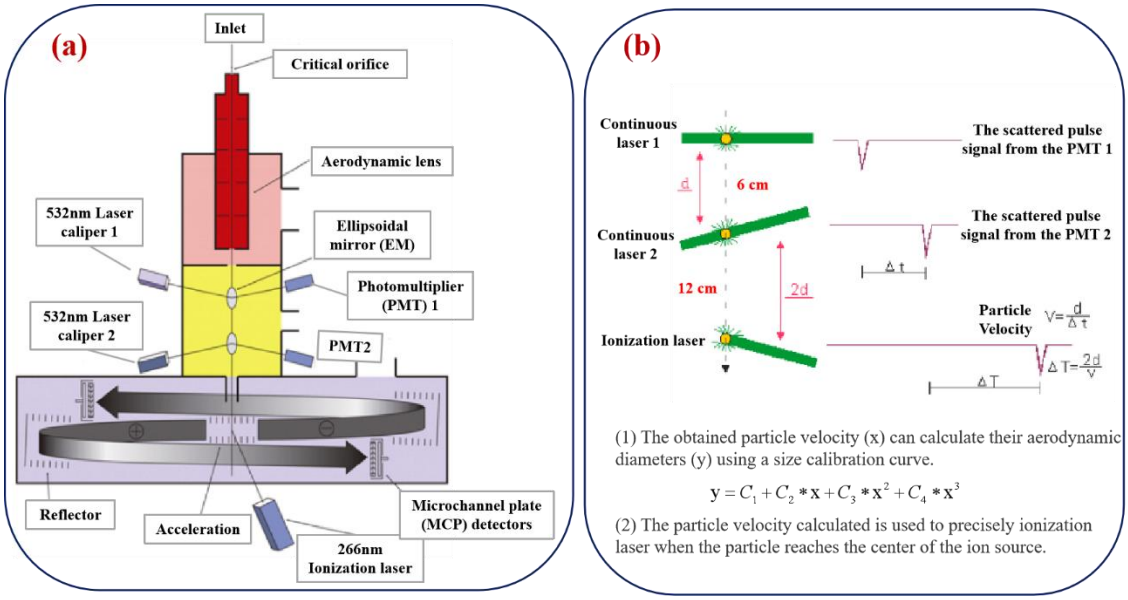

Figure R3. Schematic diagram of the SPAMS.

A publication reported that the particle-detection efficiency of the SPAMS exhibits a strong dependence on particle sizes and counts of different particle types in each size range, not absolute atmospheric concentrations (Yang et al., 2017). Although the SPAMS determines the number size distribution in a size range of 200-2000 nm, the detection efficiency is low at both ends of the size range. Therefore, quantifying the absolute contribution of each particle type to ambient particle number and mass concentration is difficult. Composition-dependent ionization efficiency and size-dependent particle detection efficiency are the predominant confounding factors (Allen et al., 2000; Reilly et al., 2000; Wenzel et al., 2003; Healy et al., 2013). The characteristics of aerodynamic size measured by SPAMS are statistical results, while the relative number fraction of different particle types in each size bin is significant. To clarify this concern, more descriptions of the size distribution using SPAMS have been added as follows.

Line 293-297:

"It should be pointed out that further application of this method would require a co-located particle-sizing instrument to scale the size-resolved particle detection efficiency. Both particle composition and size-dependent are the predominant impacting factors on the particle detection efficiency of the SPAMS (Wenzel et al., 2003; Yang et al., 2017; Healy et al., 2013)."

Reference:

Allen, J. O., Fergenson, D. P., Gard, E. E., Hughes, L. S., Morrical, B. D., Kleeman, M. J., Gross, D. S., Galli, M. E., Prather, K. A., and Cass, G. R.: Particle Detection Efficiencies of Aerosol Time of Flight Mass Spectrometers under Ambient Sampling Conditions, Environ. Sci. Technol., 34, 211–217, http://dx.doi.org/10.1021/es9904179, 2000.

Healy, R. M., Sciare, J., Poulain, L., Crippa, M., Wiedensohler, A., Prévôt, A.S.H., Baltensperger, U., Sarda-Estève, R., McGuire, M. L., Jeong, C. H., McGillicuddy, E., O'Connor, I. P., Sodeau, J. R., Evans, G. J., and Wenger, J. C.: Quantitative determination of carbonaceous particle mixing state in Paris using single-particle mass spectrometer and aerosol mass spectrometer measurements, Atmos. Chem. Phys., 13, 9479–9496, http://dx.doi.org/10.5194/acp-13-9479-2013, 2013.

Kane, D. B. and Johnston, M. V.: Size and Composition Biases on the Detection of Individual Ultrafine Particles by Aerosol Mass Spectrometry, Environ. Sci. Technol., 34, 4887–4893, https://doi.org/10.1021/es001323y, 2000.

Matthew, B. M., Middlebrook, A. M., and Onasch, T. B.: Collection Efficiencies in an Aerodyne Aerosol Mass Spectrometer as a Function of Particle Phase for Laboratory Generated Aerosols, Aerosol Sci. Technol., 42, 884–898, https://doi.org/10.1080/02786820802356797, 2008.

Wenzel, R. J., Liu, D.-Y., Edgerton, E. S., and Prather, K. A.: Aerosol time-of-flight mass spectrometry during the Atlanta Supersite Experiment: 2. Scaling procedures, J. Geophys. Res., 108, 8427, http://dx.doi.org/10.1029/2001jd001563, 2003.

Yang, J., Ma, S. X., Gao, B., Li, X. Y., Zhang, Y. J., Cai, J., Li, M., Yao, L. A., Huang, B., and Zheng, M.: Single particle mass spectral signatures from vehicle exhaust particles and the

source apportionment of on-line $PM_{2.5}$ by single particle aerosol mass spectrometry, Sci. Total Environ., 593–594, http://dx.doi.org/10.1016/j.scitotenv.2017.03.099, 2017.

Zhao, J., Du, W., Zhang, Y. J., Wang, Q. Q., Chen, C., Xu, W. Q., Han, T. T., Wang, Y. Y., Fu, P. Q., Wang, Z. F., Li, Z. Q., and Sun, Y. L.: Insights into aerosol chemistry during the 2015 China Victory Day parade: results from simultaneous measurements at ground level and 260 m in Beijing, Atmos. Chem. Phys., 17, 3215–3232, https://doi.org/10.5194/acp-17-3215-2017, 2017.

4. Since the rich-K type particles are often the dominant particle type, I am surprised that there isn't more time dedicated to describing what these particles might be. While this reviewer understands that these are clusters, the other clusters have much more intuitive names that can be traced back to certain sources. Similarly, I am surprised looking at Figure S3 that the all of the clusters have a large potassium peak. Is this usual for this SPAMS instrument?

Response: As the description shown in Supplementary Material (Text S1. Characteristics of particle composition), the particles containing the strongest potassium (*m/z* $^{39}K^+$) signal in the positive MS and significant sulfate (*m/z* $^{97}HSO_4^-$), and nitrate (*m/z* $^{46}NO_2^-$, $^{62}NO_3^-$) fragments in the negative MS are identified as Potassium-rich (rich-K) (Fig. S3a). The sources of the rich-K particles are complex, including biomass burning (Pratt et al., 2011), secondary formation (Bi et al., 2011; Shen et al., 2017), and industrial and traffic emissions (Zhang et al., 2017). A weak phosphate (*m/z* $^{79}PO_3^-$) signal is seen in Fig. S3a, consistent with the results of a study that $^{79}PO_3^-$ could be originated from motor vehicle lubricants (Yang et al., 2017). Significant peaks $^{97}HSO_4^-$ and $^{62}NO_3^-$ indicate that the rich-K particle might experience atmospheric aging after the primary biomass burning emission.

As the reviewer noted, many studies reported that SPAMS is very sensitive to alkali metal cations, and the ionization efficiencies of different chemical species are greatly varied (Gross et al., 2000; Xu et al., 2017). It should be noted that potassium with the desorption lasers used in the SPAMS could lead to its appearance in most particle types (Healy et al., 2013). SPAMS is extremely sensitive to potassium ($^{39}K^+$), thus its detection is possible even presents at a trace level such as in the exhausts of diesel- or bio-diesel-fueled vehicles (Giorio et al., 2015). Moreover, the peak at *m/z* 39 might not only be for potassium ($[K]^+$ and also for fragment $[C_3H_3]^+$ (Silva and Prather, 2000). The absence of common peaks associated with potassium (i.e. *m/z* ^{113} $[K_2Cl]^+$ and *m/z* ^{213} $[K_3SO_4]^+$), additionally of the ratio between *m/z* 39 and 41 is ~18 (the isotopic ratio for $^{39}K/^{41}K$ is 13.28), further suggest that peak at *m/z* 39 is not for potassium only, whereas it generally dominates in biomass burning particles and other potassium-containing clusters (Silva et al., 1999; Dall'Osto et al., 2012). The presences of potassium and its cluster ions with chloride and sulfate allow the definitive identification of particles derived from biomass burning, sea salt, or soil particles. The combinations of both characteristic features allow for the comprehensive identification of biomass-burning particles, isolating them from other combustion-related particles, such as tobacco smoke. Moreover, the peaks at *m/z* 45,

59, and 71 are distinctive in the biomass-burning particles. The related elaborations in Supplementary materials (Text S1) have been revised as follows.

Line 16-28 in Supplementary materials (Text S1):

"Nine particle groups are identified based on their chemical characteristics shown in the publications. General mass spectral characteristics for each particle group are presented in Fig. S3. The intense potassium ($^{39}K^+$) peak in almost all particles is attributed to the highly sensitive to potassium with the desorption laser used in the SPAMS (Gross et al., 2000; Xu et al., 2017; Giorio et al., 2015). Studies have reported that potassium by itself isn't an adequate marker for biomass burning because it presents in mass spectra of a variety of particle types (Healy et al., 2013). Moreover, the peak at m/z 39 might not be for K^+ and also for organic fragment $C_3H_3^+$ (Silva and Prather, 2000). Especially, the presence of other potassium clusters (i.e., m/z $^{113}K_2Cl^+$ or m/z $^{213}K_3SO_4^+$) and peaks at m/z 45, 59 and 71 are distinctive for biomass burning particles (Silva et al., 1999; Dall'Osto et al., 2012). The combination of the presence of phosphate (m/z $^{79}PO_3^-$) allows identification of particles derived from traffic emissions."

Reference:

Dall'Osto, M., and Harrison, R. M.: Urban organic aerosols measured by single particle mass spectrometry in the megacity of London, Atmos. Chem. Phys., 12, 4127–4142, https://doi.org/10.5194/acp-12-4127-2012, 2012.

Gross, D. S., Gälli, M. E., Siliva, P. J., and Prather, K. A.: Relative sensitivity factors for alkali metal and ammonium cations in single-particle aerosol time-of-flight mass spectra, Anal. Chem., 72, 416–422, https://doi.org/10.1021/ac990434g, 2000.

Giorio, C., Tapparo, A., Dall'Osto, M., Beddows, D. C. S., Esser-Gietl, J. K., Healy, R. M., and Harrison, R. M.: Local and Regional Components of Aerosol in a Heavily Trafficked Street Canyon in Central London Derived from PMF and Cluster Analysis of Single-Particle ATOFMS Spectra, Environ. Sci. Technol., 49(6), 3330–3340, https://doi.org/10.1021/es506249z, 2015.

Silva, P. J., Liu, D.Y., Noble, C.A., and Prather, K. A.: Size and chemical characterization of individual particles resulting from biomass burning of local Southern California species, Environ. Sci. Technol., 33, 3068–3076, https://doi.org/10.1021/es980544p, 1999.

Silva, P. J. and Prather K. A.: Interpretation of mass spectra from organic compounds in aerosol time-of-flight mass spectrometry, Anal. Chem., 72, 3553–3562, https://doi.org/10.1021/ac9910132, 2000.

Healy, R. M., Sciare, J., Poulain, L., Crippa, M., Wiedensohler, A., Prévôt, A.S.H., Baltensperger, U., Sarda-Estève, R., McGuire, M. L., Jeong, C. H., McGillicuddy, E., O'Connor, I. P., Sodeau, J. R., Evans, G. J., and Wenger, J. C.: Quantitative determination of carbonaceous particle mixing state in Paris using single-particle mass spectrometer and aerosol mass spectrometer measurements, Atmos. Chem. Phys., 13, 9479–9496, http://dx.doi.org/10.5194/acp-13-9479-2013, 2013.

Xu, J., Li, M., Shi, G., Wang, H., Ma, X., Wu, J., Shi, X., and Feng, Y.: Mass spectra features of biomass burning boiler and coal burning boiler emitted particles by single particle aerosol

mass spectrometer, Sci. Total Environ., 598, 341–352, https://doi.org/10.1016/j.scitotenv.2017.04.132, 2017.

5. Figure 2 would be greatly improved if (a) the table was not inset into the figure, and (b) that the non-Chinese countries were not plotted in blue. For part (a), it is difficult to read the text; for part (b), blue colors on maps typically denote bodies of water.

Response: Suggestion taken. The original table inserted in Figure 2 was removed, and the table inside was moved to Supplementary (Table S1). In addition, Figure 2 with the embedded chart has been redrawn as below.

"Table S1. Number concentration and relative fraction of the six main particle types in four trajectory clusters during the whole observation."

Type	Cluster 1		Cluster 2		Cluster 3		Cluster 4	
	Counts	Fraction (%)	Counts	Fraction (%)	Counts	Fraction (%)	Counts	Fraction (%)
rich-K	103275	32.7	1486	30.8	33319	26.8	4291	25.2
BB	58379	18.5	1731	35.9	23970	19.3	4562	26.8
OC	37856	12.0	744	15.4	19227	15.5	2138	12.5
Ammonium	39388	12.5	240	5.0	12948	10.4	1304	7.7
EC-aged	35143	11.1	245	5.1	9553	7.7	1077	6.3
Dust	28002	8.9	176	3.6	20613	16.6	2827	16.6

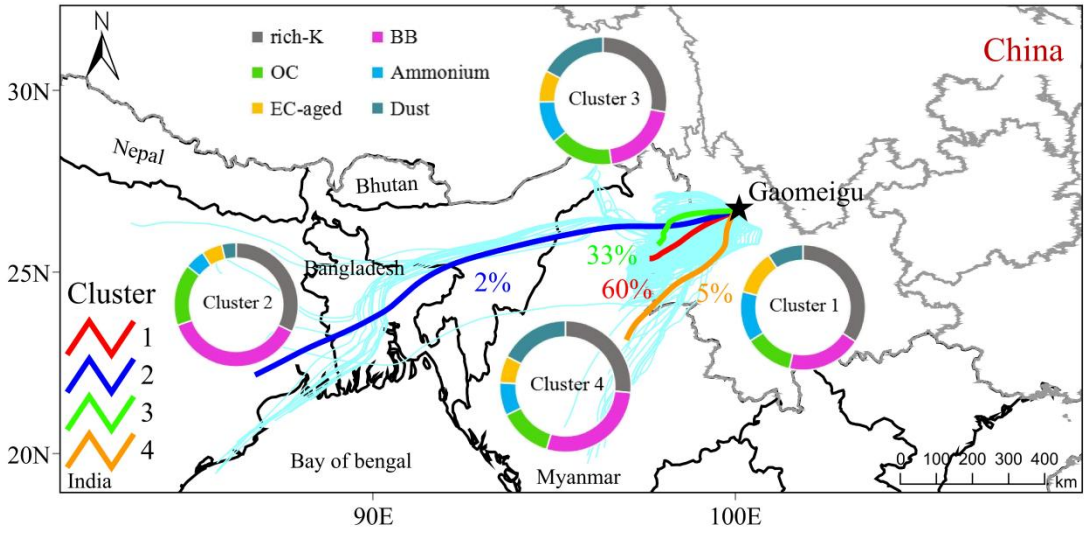

Figure 2. Maps of the mean HYSPLIT back trajectory clusters (72 h) at the height of 500 m during the whole field observation. Embedded pie chart represents the relative fraction of each particle type in the four clusters.

6. How are the errors bars generated for the particle types in each cluster in Figure 2?

Response: Figure 2 has been modified with the Comment 5. In original manuscript, the counts in Figure 2 are calculated by the average of the number concentration of each particle type during the total sampling periods for each cluster. In the revised manuscript, the counts have been changed to the ratio of the sum number concentration of each particle type to the sum of the total particle number in each cluster. The error bars are thus removed. The update of the relevant values shown in Table S1 with the Comment 5.

7. It might be useful to put the y-axis on Figure 3a, Figure 5a, and Figure 5b on a log scale. Mainly, I was interested in seeing how many particles there are of each type at the larger sizes where the number fraction plots get a little noisy.

Response: The new Figure R4a (original Figure 3a) put the y-axis on a log scale. There are relatively fewer particles with larger sizes for each particle type. For example, most count numbers are <100 at the size >1.2 μm, except for Dust. Especially, in new Fig. R4b and c, the particles with sizes >1.2 μm could not be seen due to the extremely small count number during Episodes 1 and 2.

Studies have reported that the SPAMS instrument is more sensitive to relatively small size particles. The higher sensitivity to chemical species with smaller particle sizes is attributed to (1) a greater volume fraction of small particles being vaporized by the ablation/ionization laser and (2) a lower probability of positive-negative charge recombination in the ablation plume for smaller-size particles (Bhave et al., 2002; Noble and Prather, 2000).

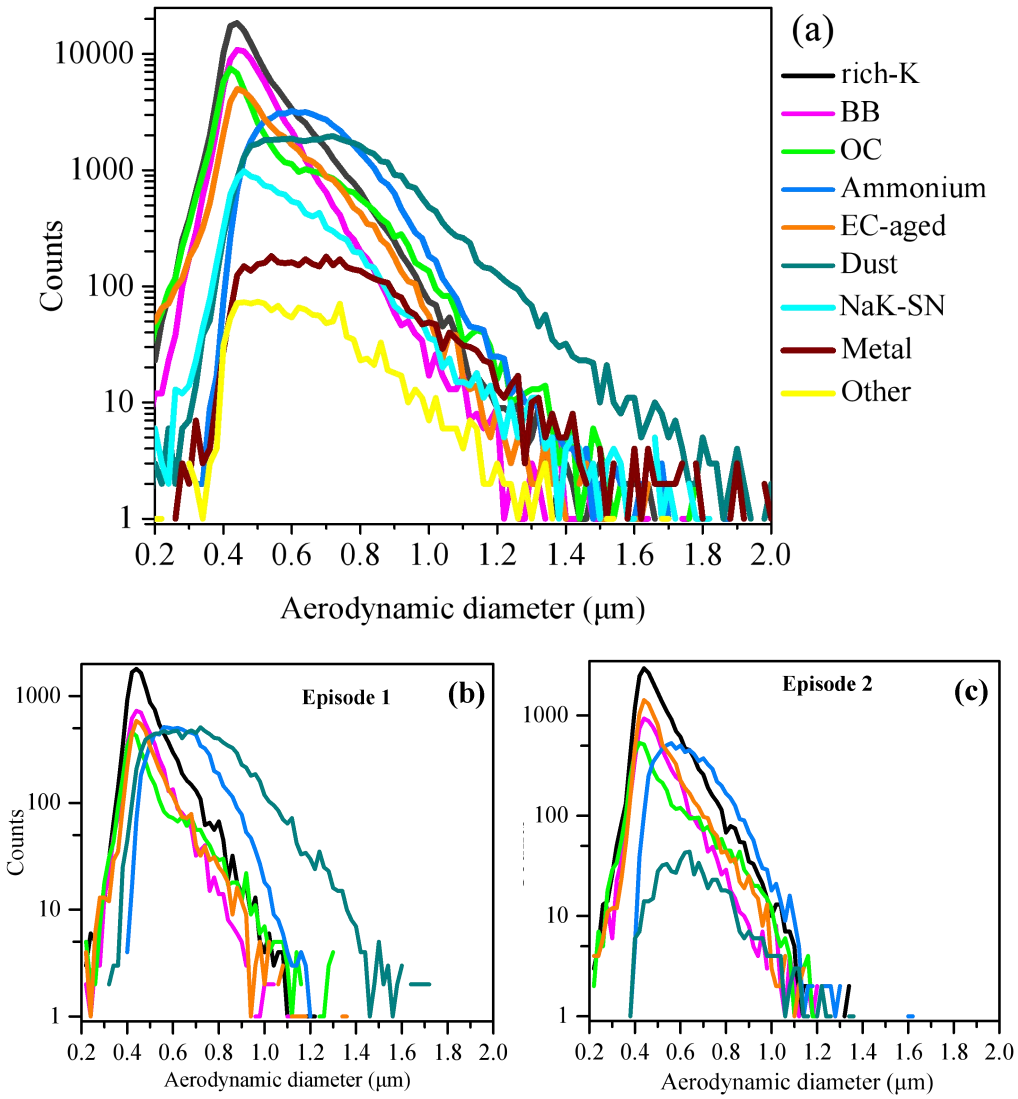

Figure R4. Size distributions of the particle count for nine particle types during the entire sampling campaign (a), and for major particle types during Episode 1 (b) and Episode 2 (c).

The particles with relatively lower concentrations also show a minor influence on the overview of size distribution. Since the size distributions of single particles from SPAMS are not scaled by other instruments such as SMPS, we have reduced the descriptions of the particle sizes in Section 3.2. In addition, as the count numbers with larger particle sizes fluctuate greatly after using a log scale of the y-axis, it might be reasonable and aesthetic to keep the y-axis intact.

Reference:

Bhave, P. V., Allen, J. O., Morrical, B. D., Fergenson, D. P., Cass, G. R., and Prather, K. A.: A Field-Based Approach for Determining ATOFMS Instrument Sensitivities to Ammonium and Nitrate, Environ. Sci. Technol., 36, 4868–4879, https://doi.org/10.5194/acp-12-4127-2012, 2002.

Noble, C. A., and Prather, K. A.: Real-time single particle mass spectrometry: A historical review of a quarter century of the chemical analysis of aerosols, Mass Spec. Rev., 19, 248–274, https://doi.org/10.1002/1098-2787(200007)19:4<248::AID-MAS3>3.0.CO;2-I, 2000.

8. Figure 7 suggests that knowing the oxidant concentration is not enough a priori knowledge to know the number fraction of particles that contain markers for secondary aerosol. Thus, you are missing some dimension that can make this analysis useful. Potentially, you are in an oxidant limited regime sometimes, and a precursor limited regime in other times. Perhaps also peak heights would be more useful than fraction containing, and could help tighten up the relationships.

Response: As shown in Fig. R5, the peak areas of each secondary ion ($^{43}C_2H_3O^+$, $^{89}HC_2O_4^-$, $^{18}NH_4^+$, $^{62}NO_3^-$, and $^{97}HSO_4^-$) are positively correlated with the concentrations of oxidant (O_x) during E2. However, there is no uniform linear correlation during E1.

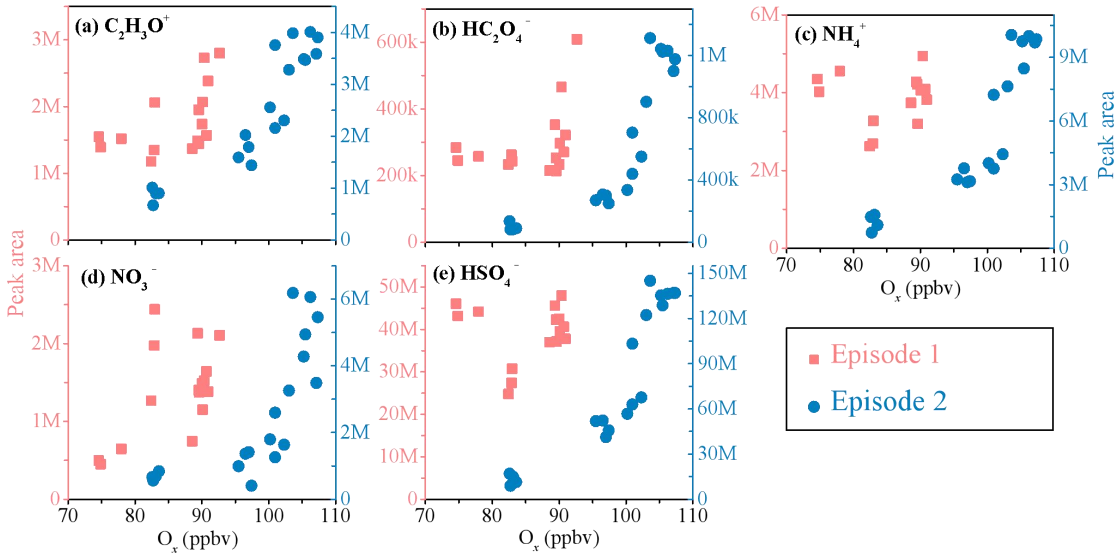

Figure R5. Correlations between the peak area (PA) for five secondary ions and O_x concentration during Episodes 1 and 2. The k and M represents thousands and ten thousands in the y-axis, respectively.

SPAMS has been made in quantifying individual chemical species either through multivariate analysis or by applying peak intensities for specific ions (e.g., Healy et al., 2013; Jeong et al., 2011; Xing et al., 2011). However, the ionization efficiency of different chemical species is difficult due to the variations in their ionization energies (Gross et al., 2000; Xu et al., 2017). Therefore, compared to absolute count number and peak area, number fraction, or relative peak area (RPA) are commonly applied because they are less sensitive to the variability in ion intensities associated with particle-laser interactions (Gross et al., 2000; Zhang et al., 2014; Zhang et al., 2020). Specifically, highly sensitive ions during the ionization could lead to a relatively higher peak area, and thus lower the RPA of other ion peaks.

RPA, defined as the peak area of each *m/z* divided by the total dual ion mass spectral peak area, is related to the relative amount of a species on a particle. To avoid the situation where the high peak area of some ions with high ionization efficiency (e.g., $^{39}K^+$) reduces the RPA of other ions, we tend to select the number fraction of $^{43}C_2H_3O^+$, $^{89}HC_2O_4^-$, $^{62}NO_3^-$, $^{97}HSO_4^-$, and $^{18}NH_4^+$-containing particles to investigate secondary formation mechanism.

Reference:

Gross, D. S., Gälli, M. E., Siliva, P. J., and Prather, K. A.: Relative sensitivity factors for alkali metal and ammonium cations in single-particle aerosol time-of-flight mass spectra, Anal. Chem., 72, 416–422, https://doi.org/10.1021/ac990434g, 2000.

Healy, R. M., Sciare, J., Poulain, L., Crippa, M., Wiedensohler, A., Prévôt, A.S.H., Baltensperger, U., Sarda-Estève, R., McGuire, M. L., Jeong, C. H., McGillicuddy, E., O'Connor, I. P., Sodeau, J. R., Evans, G. J., and Wenger, J. C.: Quantitative determination of carbonaceous particle mixing state in Paris using single-particle mass spectrometer and aerosol mass spectrometer measurements, Atmos. Chem. Phys., 13, 9479–9496, http://dx.doi.org/10.5194/acp-13-9479-2013, 2013.

Jeong, C. H., McGuire, M. L., Godri, K. J., Slowik, J. G., Rehbein, P.J.G., and Evans, G.J.: Quantification of aerosol chemical composition using continuous single particle measurements. Atmos. Chem. Phys., 11, 7027–7044, http://dx.doi.org/10.5194/acp-11-7027-2011, 2011.

Liang, Z. C., Zhou, L. Y., Infante C.R.A., Li, X. Y., Cheng, C. L., Li, M., Tang, R. Z., Zhang, R. F., Lee, P.K.H., Lai, A.C.K., and Chan, C. K.: Sulfate Formation in Incense Burning Particles: A Single-Particle Mass Spectrometric Study, Environ. Sci. Technol. Lett., 9, 718–725, https://doi.org/10.1021/acs.estlett.2c00492, 2022.

Xing, J. H., Takahashi, K., Yabushita, A., Kinugawa, T., Nakayama, T., Matsumi, Y., Tonokura, K., Takami, A., Imamura, T., Sato, K., Kawasaki, M., Hikida, T., Shimono, A.: Characterization of aerosol particles in the Tokyo Metropolitan area using two different particle mass spectrometers. Aerosol Science and Technology 45, 315–326, http://dx.doi.org/10.1080/02786826.2010.533720, 2011.

Xu, J., Li, M., Shi, G. L., Wang, H. T., Ma, X., Wu, J. H., Shi, X. R., and Feng, Y. C.: Mass spectra features of biomass burning boiler and coal burning boiler emitted particles by single particle aerosol mass spectrometer, Sci. Total Environ., 598, 341–352, https://doi.org/10.1016/j.scitotenv.2017.04.132, 2017.

Zhang, G. H., Lian, X. F., Fu, Y. Z., Lin, Q. H., Li, L., Song, W., Wang, Z. Y., Tang, M. J., Chen, D. H., Bi, X. C., Wang, X. M., and Sheng, G. Y.: High secondary formation of nitrogen-containing organics (NOCs) and its possible link to oxidized organics and ammonium, Atmos. Chem. Phys., 20, 1469–1481, https://doi.org/10.5194/acp-20-1469-2020, 2020.

9. Figure 8 is interesting because the trends are similar between the episodes; however, that they don't line up makes the interpretation difficult. Again, it seems that you're missing some dimension here that could help your

analysis—perhaps some smarter filtering by particle type could help? As it stands, the interpretation is muddled.

Response: As shown in Fig. R6, higher RH is seen RH during E1 (ranging from 37 to 99%) than E2 (25-77%). The aqueous-phase formation pathways of secondary species could be represented by the correlations between the number fraction of each secondary species and RH during nighttime (from 20:00 to 06:00 the next day) in the two episodes. During the nighttime, RH ranges from 79 to 99% in E1, and 43 to 77% in E2. Therefore, Fig. 7 is not suitable to be a line-up.

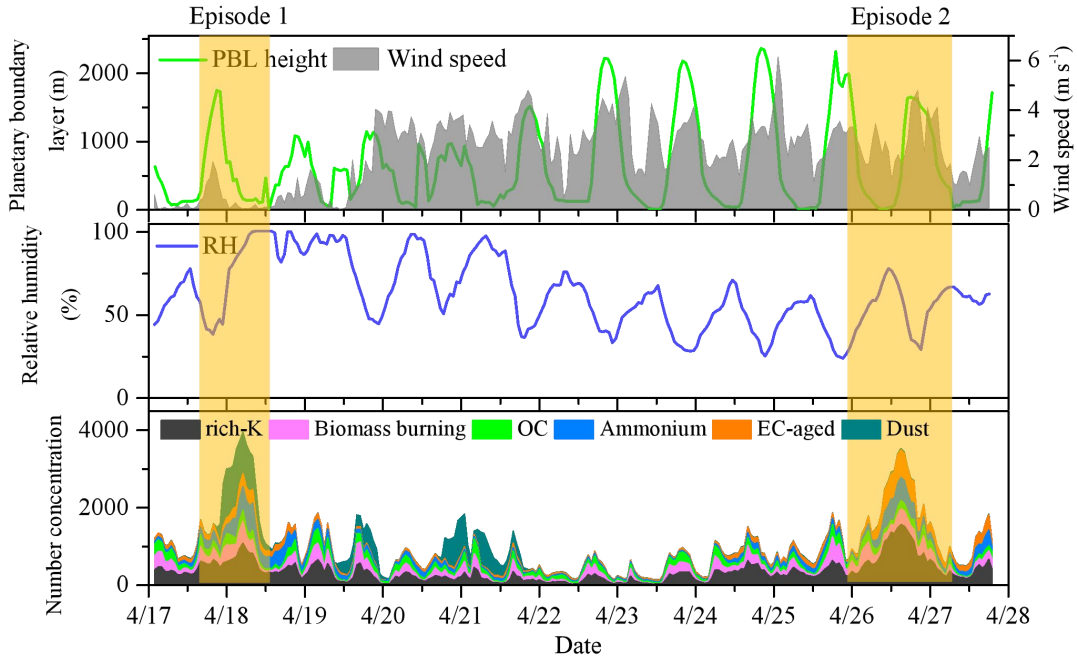

Figure R6. Time-series plots of PBL height, wind speed, relative humidity (RH), and the number concentration of the main six particle groups. Yellow shades correspond to Episodes 1 and 2, respectively.

It should be noted that it is still quite challenging for SPAMS to provide quantitative information on chemical compositions. Despite this, the number fraction and relative peak area (RPA) are still reliable indicators for investigating the atmospheric processing of various species in individual particles. Although they are insufficient to provide a quantitative assessment of secondary formation, our results successfully provide evidence for the possible pathways of secondary production in the southeastern margin of TP and, thus, can help achieve a qualitative understanding of the formation and evolution of secondary species in individual particles (Lian et al., 2021).

In addition, the reason for choosing the number fraction over the peak area in the presentation is provided in Comment 8. The correlation between peak area and RH also show in Fig. R7.

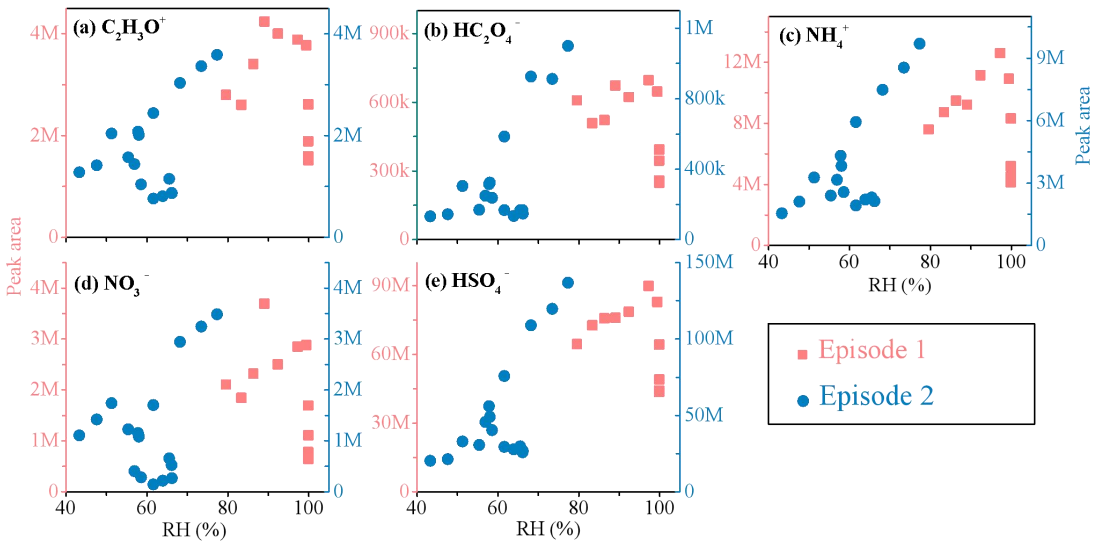

Figure R7. Correlations between the peak area (PA) for five secondary ions and RH during Episodes 1 and 2.

As per the reviewer's comment, Fig. R8 and R9 have been created. The number fractions of secondary ions are obtained by taking the percentage of the number concentration of each secondary ions in the whole detected particles. Moreover, the fraction of each particle type is also given by the ratio of the number concentration of each particle type to the whole detected particle. The mixing states are calculated by the ratio of the number concentration of secondary ions to each particle type. Therefore, both Fig. R8 and R9 could present their mixing states.

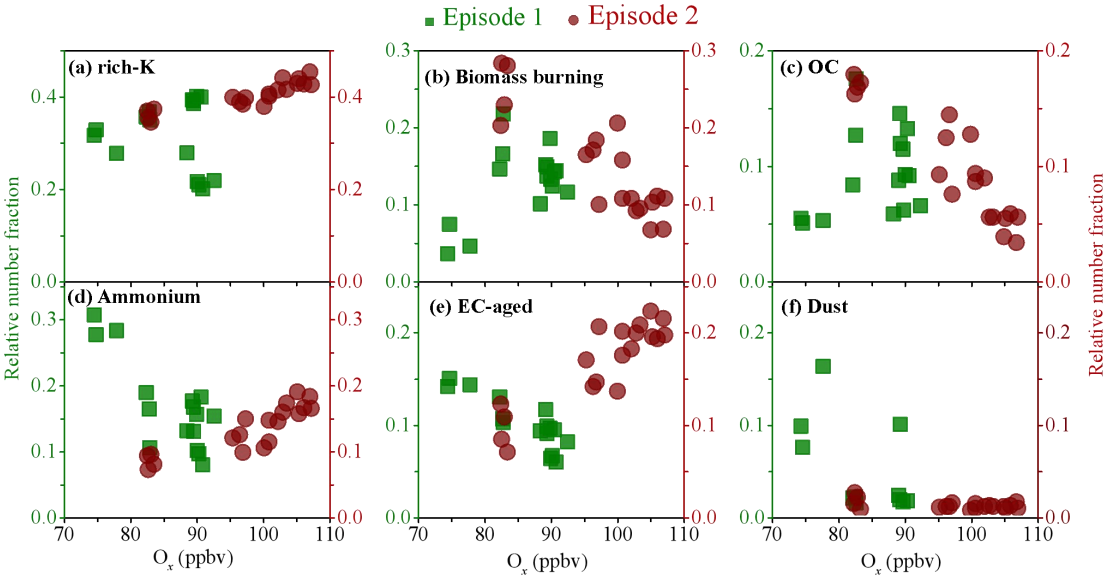

Figure R8. Correlation between the number fraction of the six particle types and O_x concentration during Episodes 1 and 2.

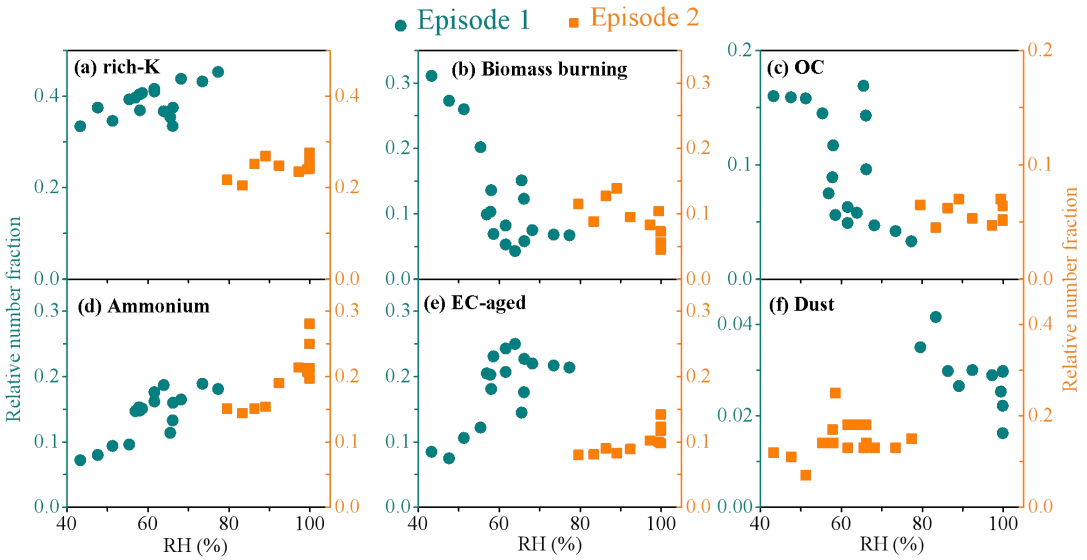

Figure R9. Correlations between the number fraction of the six particle types and RH during Episodes 1 and 2.

As discussed in Comment 8, we tend to select the number fraction. A more detailed interpretation of the aqueous-phase reaction of secondary species in TP has been clarified as follows.

Line 406-440:

"Fig. 7 illustrates that the number fractions of $^{43}C_2H_3O^+$, $^{89}HC_2O_4^-$, $^{97}HSO_4^-$, and $^{18}NH_4^+$ have moderate to strong positive correlations with RH (r = 0.70~0.81, p < 0.01 or 0.05) in the nighttime during the two episodes, except that $^{43}C_2H_3O^+$ during E2 (p = 0.48) and $^{89}HC_2O_4^-$ during E1 (p = 0.12). Furthermore, $^{62}NO_3^-$ fraction has no obvious changes with insignificant correlation with RH during E1 (p = 0.43) and presents a moderate negative correlation with RH (r = 0.69, p < 0.01) during E2. As shown in Fig. 7e, the highest aqueous formation rate of HSO_4^- is mainly due to the properties of low volatile and high hygroscopic sulfate (Wang et al., 2016; Zhang et al., 2019c; Sun et al., 2013). Compared with that during E2 (slop=0.014), the decreased formation rate of HSO_4^- during the E1 (slop=0.009) may be because of the decreases of aerosol acidity in higher RH > 80% (Huang et al., 2019; Meng et al., 2014; Tian et al., 2021). And the increased contributions of regional transport due to the high WS (2.4 ± 0.8 m s^{-1}) during E2 are comparable to the low WS (0.08 ± 0.08 m s^{-1}) during E1 (Fig. S8). The fair production rate of NH_4^+ during the E1 (slop=0.005) and E2 (slop=0.006) demonstrate that an aqueous-phase reaction could effectively promote ammonium formation. Meanwhile, a slightly larger slop during E2 could be also affected by the increased contributions of regional transport. Compared with those during E1, the inverse generation rates of two secondary organic species (i.e., $C_2H_3O^+$ and $HC_2O_4^-$) during E2 are possibly caused by the different formation pathways with a variety of RH levels or distinct regional transports. For example, $C_2H_3O^+$ shows a strong correlation with RH (r = 0.70, p < 0.05) during E1 (slop=0.003)

but has an insignificant correlation during E2. This could be explained by high RHs that could effectively promote secondary organic formation during E1. In addition, the $HC_2O_4^-$ fraction increases slightly (9.7-13.1%) during E1 is potentially ascribed to more abundant Dust-type particles (20.3%) which compose of high calcium (Ca) (Fig. S13) that favor the formation of metal oxalate complexes (i.e., Ca oxalate). At high RHs (93.4 ± 7.6%), if oxalate ions are dissolved in the aqueous phase with the presence of Ca ions, the Ca oxalate complexes can precipitate because of their low hygroscopic and insoluble natures (Furukawa and Takahashi, 2011). This could offset the oxalate formation in the aqueous-phase reaction. However, significant linear increases (slop is 0.003) with RH ($r = 0.81$, $p < 0.01$) during E2 demonstrate that the aqueous-phase reaction effectively promotes the oxalate formation (Cheng et al., 2017; Meng et al., 2020). No obvious change and insignificant correlation between $^{62}NO_3^-$ and RH are found during E1, potentially attributed to the decreases of NO_2 concentration (3.7 ± 0.4 ppbv) in the local atmosphere. Meanwhile, high RHs could promote organonitrates formation (Fang et al., 2021; Fry et al., 2014). The linearity between $^{62}NO_3^-$ and RH ($r = 0.69$, $p < 0.01$) significantly decreases during E2, mostly due to the losses of the volatile compound through the regional transport (Fig. S14).”

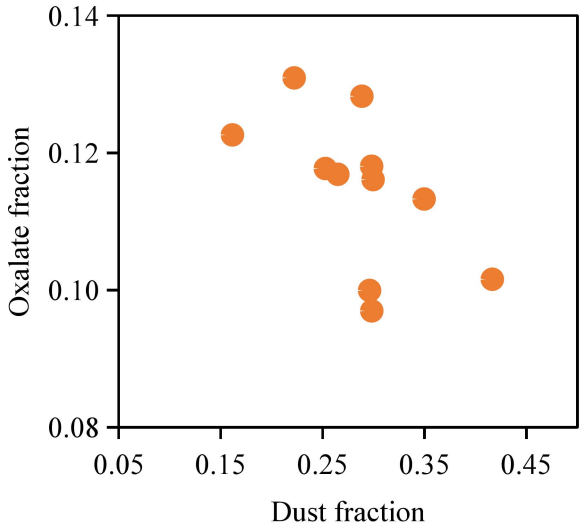

Figure S13. Correlations between the relative fraction of oxalate and Dust type during E1.

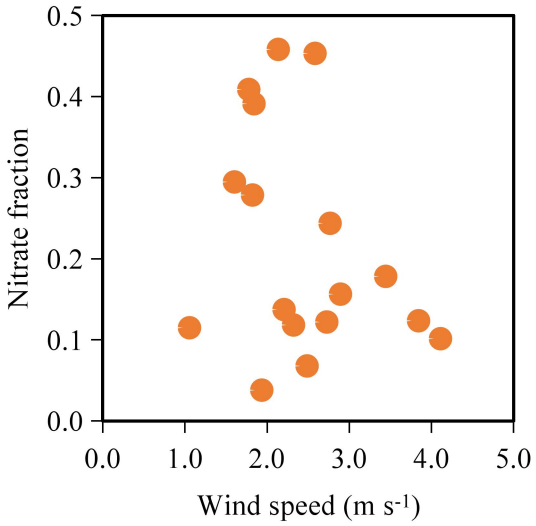

Figure S14. Correlations between the relative fraction of nitrate (62NO3−) and wind speed during E2.

Reference:

Furukawa, T., and Takahashi, Y.: Oxalate metal complexes in aerosol particles: implications for the hygroscopicity of oxalate-containing particles. Atmos. Chem. Phys., 11, 4289–4301, https://doi.org10.5194/acp-11-4289-2011, 2011.

Huang, X. J., Zhang, J. K., Luo, B., Luo, J. Q., Zhang, W., and Rao, Z. H.: Characterization of oxalic acid-containing particles in summer and winter seasons in Chengdu. China, Atmos. Environ., 198, 133–141. https://doi.org/10.1016/j.atmosenv.2018.10.050, 2019.

Lian, X. F., Zhang, G. H., Yang, Y. X., Lin, Q. H., Fu, Y. Z., Jiang, F., Peng, L., Hu, X. D., Chen, D. H., Wang, X. M., Peng, P. A., Sheng, G. Y., and Bi, X. H.: Evidence for the Formation of Imidazole from Carbonyls and Reduced Nitrogen Species at the Individual Particle Level in the Ambient Atmosphere. China, Environ. Sci. Technol. Lett., 8, 9−15. https://dx.doi.org/10.1021/acs.estlett.0c00722, 2021.